Enhanced piezoelectric effect of relaxor ferroelectrics in nonpolar direction

L.-F. Wang and J.-M. Liu[a)]
Laboratory of Solid State Microstructures, Nanjing University, Nanjing 210093, China and International Center for Materials Physics, Chinese Academy of Sciences, Shenyang 110016, China

(Received 16 November 2006; accepted 10 January 2007; published online 7 February 2007)

The polarization and electromechanical behaviors of relaxor ferroelectrics (RFs) are simulated by numerically solving the time-dependent Landau-Ginzburg equation based on a phenomenological dipole defect model. In comparison with normal ferroelectric lattice, the RF lattice shows significantly enhanced piezoelectric response along the nonspontaneous polarization axis. The evolution of dipole configuration suggests that this behavior is ascribed to the 90° flips of small-sized "super-ferroelectric" clusters induced by dipole defects. © *2007 American Institute of Physics*. [DOI: 10.1063/1.2472526]

Relaxor ferroelectrics (RFs) with ultrahigh piezoelectric performance have been a focus in last decades.[1,2] Recently, experiments on doped RFs underwent an accelerated growth, including doped $Pb(Zr_xTi_{1-x})O_3$,[3,4] doped $Pb(Zr_xNb_{1-x})O_3$ (PZN),[5] doped $Pb(Mg_xNb_{1-x})O_3-PbTiO_3$,[6,7] and doped PZN-PT.[8–12] It was shown that the piezoelectric property along nonspontaneous polar (NSP) axis can be enhanced by defect doping, accompanied by increased squareness in strain-electrical field hysteresis and decreased electric field at which the field-induced strain increases sharply.[10,11] These unusual piezoelectric responses have not yet been well understood, while current theory suggests that dipole defects usually pin ferroelectric domain walls from responding to external field.[13] In this letter, we propose an alternative explanation on these unusual piezoelectric behaviors by investigating the dipole defect model based on Landau-Ginzburg-Devonshire theory, which was employed to explain a series of phenomena associated with RFs.[14–17]

It is well established that for a ferroelectric lattice, the free energy functional F dependent on polarization $\boldsymbol{P}(\boldsymbol{r})$ and displacement $\boldsymbol{u}(\boldsymbol{r})$ is[18]

$$F[\mathbf{P}(\mathbf{r}),\mathbf{u}(\mathbf{r})]=\int_{\Omega}(f_{\mathrm{Ld}}+f_g+f_u+f_{\mathrm{es}}+f_E)d\mathbf{r}, \tag{1}$$

where f_{Ld}, f_g, f_u, f_{es}, and f_E are the Landau potential, gradient energy, elastic energy, electrostrictive interaction, and static electric energy, respectively. We consider a two-dimensional square ferroelectric lattice in x-y plane with periodic boundary conditions. The Landau potential is

$$f_{\mathrm{Ld}}(\mathbf{P}(\mathbf{r}))=A_1(P_x^2+P_y^2)+A_{11}(P_x^4+P_y^4)+A_{12}P_x^2P_y^2 +A_{111}(P_x^6+P_y^6)+A_{112}(P_x^4P_y^2+P_y^4P_x^2), \tag{2}$$

where A_1, A_{11}, A_{12}, A_{111}, A_{112} are the energy coefficients. $A_1<0$ and $A_{11}<0$ for ferroelectrics of first-order transitions. Assuming continuous variation of polarization field across domain walls, f_g is associated with the gradients of polarization field, whose lowest order with cubic symmetry is

$$f_g(P_{i,j})=\frac{1}{2}[G_{11}(P_{x,x}^2+P_{y,y}^2)+G_{12}P_{x,x}P_{y,y}+G_{44}(P_{x,y}+P_{y,x})^2+G'_{44}(P_{x,y}-P_{y,x})^2], \tag{3}$$

where $P_{i,j}=\partial P_i/\partial r_j$ and coefficients G_{11}, G_{12}, G_{44}, G'_{44} are all positive. As the first approximation, the elastic energy f_u takes

$$f_u(u_{i,j})=\frac{1}{2}C_{11}(u_{x,x}^2+u_{y,y}^2)+C_{12}u_{x,x}u_{y,y}+\frac{1}{2}C_{44}u_{x,y}^2, \tag{4}$$

where $u_{ii}=\partial u_i/\partial r_i$, $u_{i,j}=\partial u_j/\partial r_i+\partial u_i/\partial r_j (i\neq j)$, and C_{ij} is the elastic coefficient. The electrostrictive interaction f_{es} is

$$f_{\mathrm{es}}(u_{i,j},\mathbf{P}(\mathbf{r}))=-u_{x,x}\eta_{xx}-u_{y,y}\eta_{yy}-u_{x,y}\eta_{xy}, \tag{5}$$

with strain $\eta_{xx}=Q_{11}P_x^2+Q_{12}P_y^2$, $\eta_{yy}=Q_{11}P_y^2+Q_{12}P_x^2$, and $\eta_{xy}=Q_{44}P_xP_y$, where Q_{ij} are the electrostrictive coefficients. The static electric energy is simply $f_E=-\boldsymbol{E}\cdot\boldsymbol{P}$ with electric field $\boldsymbol{E}$.

The ferroelectric lattice is doped with randomly distributed dipole defects, resulting in a RF lattice. The defects change the stability of local dipoles by imposing fluctuations to A_1 in Eq. (2) as $A_1(\boldsymbol{r})'=A_1+b_mc(\boldsymbol{r})$, where b_m taking its value randomly within $[-b_M,b_M]$ characterizes the influence of defects on dipole stability. Variable c $(c=0,1)$ labels the defect state of a site, $c=1$ refers to a defective site, and $c=0$ refers to a perfect dipole site. A positive or negative b_m means that a defect enhances or suppresses the local dipole moment of a lattice site. The concentration of dipole defects is C_0, and C_p measures the density of defects with $b_m>0$.

We simulate the temporal evolution of local $\boldsymbol{P}$ and $\boldsymbol{u}$ by solving a coupled set of time-dependent Ginzburg-Landau (TDGL) equations:

$$\partial P_i(\mathbf{r},t)/\partial t=-L_P\delta F/\delta P_i(\mathbf{r},t),\quad \partial u_i(\mathbf{r},t)/\partial t=-L_u\delta F/\delta u_i(\mathbf{r},t)\quad (i=x,y), \tag{6}$$

where L_P and L_u are the kinetic coefficients for $\boldsymbol{P}$ and $\boldsymbol{u}$, respectively. $L_P=L_u$ and the same time scale for the evolution of $\boldsymbol{P}$ and $\boldsymbol{u}$ can be applied since we only simulate the quasistatic behavior in the infinitely slow limit. The calculation is performed via Euler algorithm by a finite difference scheme for spatial and time derivatives in the $L\times L$ lattice, with lattice spacing $\Delta L=1.0$ and time step $\Delta t=0.001$ for nu-

a)Author to whom correspondence should be addressed; electronic mail: liujm@nju.edu.cn

TABLE I. Parameters chosen for the simulation.

A_1	A_{11}	A_{12}	A_{111}	A_{112}	G_{11}
−1.00	−0.24	−2.50	0.49	1.20	1.60
G_{12}	G_{44}	G'_{44}	C_{11}	C_{12}	C_{44}
0.00	0.8	0.8	2.75	1.79	0.54
Q_{11}	Q_{12}	Q_{44}	C_p	b_M	L
0.142	−0.0074	0.0157	0.50	25.00	72

merical stability. We initial the lattice by employing the scheme reported earlier.[19] Other parameters for simulation are listed in Table I, which are chosen to simulate tetragonal ferroelectrics with SP axis along ⟨10⟩,[18] while the temperature is much lower than the Curie point, which will not be considered in the simulation. The data presented below are taken after a sufficiently long-time evolution of the lattice towards the equilibrium dipole configurations.

In Fig. 1 the simulated domain patterns for a normal ferroelectric (NF) lattice (C_0=0, left column) and a RF lattice (C_0=0.3 and C_p=0.5, right column) at different $\boldsymbol{E}$ along the NSP axis [11] ($E^{[11]}$) are presented, where the colors

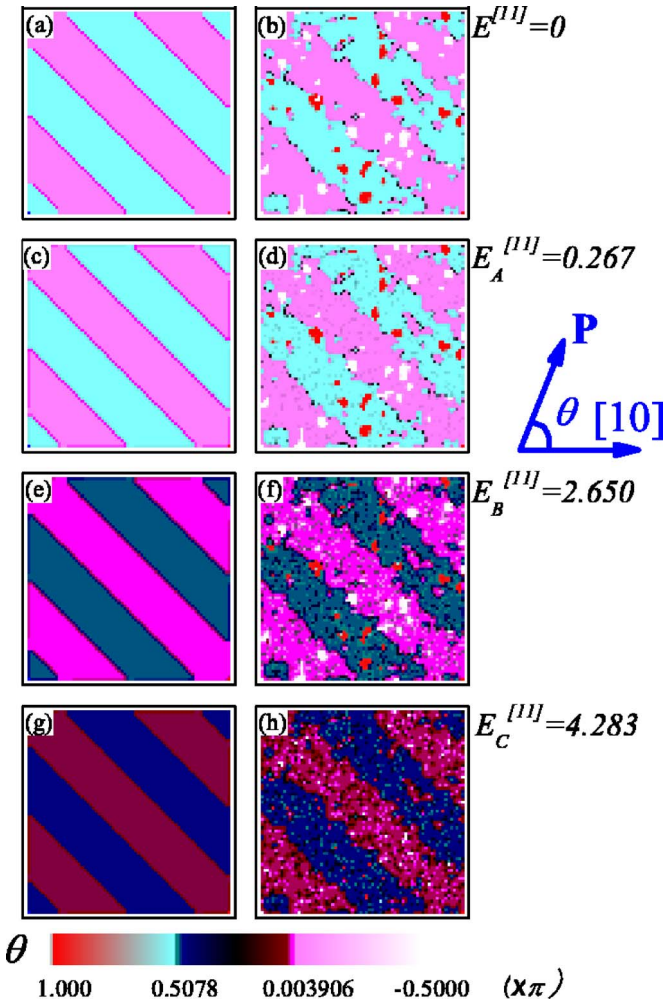

FIG. 1. (Color online) Simulated domain patterns for C_0=0 (left column) and C_0=0.3 (right column) at different electric field $E^{[11]}$. The colors represent different orientations of the domains, as defined by the color bars (angle θ).

represent the domain dipole orientations. At $E^{[11]}=0$ and $C_0=0$ [Fig. 1(a)], a typical twin-domain configuration is shown, with dipole orientations along [10] and [01] ($\theta=0$ and $\pi/2$). The 90° walls are smooth and all dipoles within the domains have similar moment. For RF lattice shown in Fig. 1(b), the stripelike domain pattern is roughly retained although the walls become irregular and many clusterlike tiny domains are embedded in the matrix of FE domains along [10] and [01]. These tiny-sized domains may align along various orientations. Typically, tiny domains with [01] and $[0\bar{1}]$ orientations embedded inside the [10] stripe domains and those with [10] and $[\bar{1}0]$ orientations inside the [01] stripe domains.

As mentioned above, two types of defects with $b_m>0$ and $b_m<0$, respectively, are doped into the lattice. As $b_m>0$, the local site dipole is suppressed, inducing tiny-sized paraelectric regions (PERs). As $b_m<0$, the local site dipole is enhanced, generating small-sized "super-ferroelectric" regions (SFRs) in the lattice. These SFRs are crucial to the unusual piezoelectric behavior of the lattice along the NSP axis, as shown below.

To investigate the piezoelectric response of the NSP [111] axis, we apply electric field $E^{[11]}$ along axis [11]. At small ($E^{[11]}<0.267$), the domains for both the NF and RF lattices are stable and no dipole aligning along [11] is observed, as shown in Figs. 1(c) and 1(d). However, a rectangle-rhombic phase transition takes place upon further increasing of $E^{[11]}$ up to 2.650, as shown in Fig. 1(e) where the stripe domains have a rotation of 3.5° from ⟨10⟩ axis towards [11] axis for the NF lattice, while for the RF lattice those small PERs become almost completely polarized along axis [11] and those SFRs still remain aligned along ⟨10⟩, evidenced with Fig. 1(f). As $E^{[11]}=4.283$, for the NF lattice, the stripe domains have an averaged rotation of ~7.1° toward [11] axis, as shown in Fig. 1(g). For the RF lattice, the stripe domains also rotate ~7.1°. However, those SFRs rotate an angle of ~90° in an abrupt manner to be aligned in the same direction as the stripe domains. Only some very stable SFR seeds retain against the rotation, as shown in Fig. 1(h). It should be mentioned here that given a $E^{[11]}$, the stripe domains for both the NF and RF lattices have similar rate of rotation.

The domain evolutions revealed above allow us to argue the possible difference in piezoelectric response between the NF and RF lattices. In Fig. 2(a), we show the average polarization component along [11] axis, $P^{[11]}$, and the average electric-induced transverse strain $\Delta\eta_{11}^{[11]}=\langle\eta_{11}^{[11]}(E)\rangle-\langle\eta_{11}^{[11]}\times(E=0)\rangle$ as a function of $E^{[11]}$ for the two lattices, where η_{11} is defined as $\eta_{11}=(\eta_{xx}+\eta_{yy+}\eta_{xy})/2$. The longitudinal piezoelectric coefficient $d_{33}^{[11]}$, defined as the slope of $\Delta\eta_{11}^{[11]}$ as a function of $E^{[11]}$, is represented in Fig. 2(b). For NF lattice, $P^{[11]}$ has a nonzero value at zero field due to coexisting domains and it has a roughly linear dependence on $E^{[11]}$, $\Delta\eta_{11}^{[11]}$ is also a linear function of $E^{[11]}$. The $d_{33}^{[11]}\sim E^{[11]}$ curve shows the first broad peak (peak I) at $E^{[11]}=E_A^{[11]}\approx 0.32$, indicating the rectangle-rhombic phase transition. The corresponding domain pattern in prior to this transition is shown in Fig. 1(c). After this transition, $P^{[11]}$ and $\Delta\eta_{11}^{[11]}$ increase while $d_{33}^{[11]}$ decrease smoothly with increasing $E^{[11]}$, corresponding to the continuous rotation of the stripe domains to [11] axis, as shown in Figs. 1(e) and 1(g).

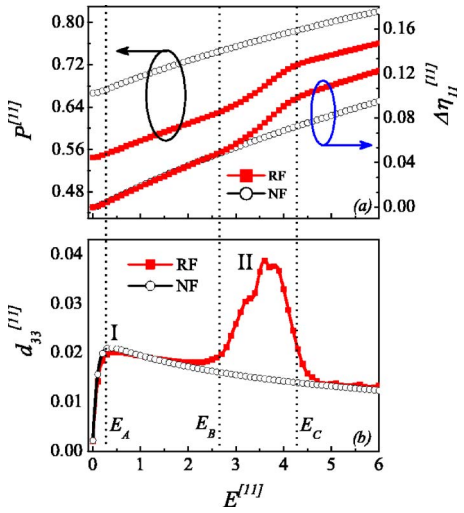

FIG. 2. (Color online) (a) Averaged polarization $P^{[11]}$ and averaged transverse strain $\Delta\eta_{11}^{[11]}$, and (b) longitudinal piezoelectric coefficient $d_{33}^{[11]}$ as a function of electric field $E^{[11]}$, for NF lattice and RF lattice.

However, more complex behaviors are observed for the RF lattice. At $E^{[11]}=0$, $P^{[11]}$ is slightly smaller than that of the NF lattice due to the dipole defects. Peak I is also slightly lower than that of the NF lattice because those SFRs remain stable against rotation toward the [11] axis. Within the window from $E_A^{[11]}=0.32$ to $E_B^{[11]}=2.650$, $P^{[11]}$ increases at the same rate approximately and $\eta_{11}^{[11]}$ does not show large differences in comparison with those for the NF lattice. Within the window from $E_B^{[11]}=2.650$ to $E_C^{[11]}=4.283$, the growth of $P^{[11]}$ in response to increasing $E^{[11]}$ is steeper and the domain evolution is shown in Figs. 1(f) and 1(h), where the SFRs flip to the same orientations as the stripe domains. This sequence generates extra strain, which corresponds to sharp increasing of the transverse strain $\Delta\eta_{11}^{[11]}$ and thus peak II at $E^{[11]}\sim 3.67$ in the plot of $d_{33}^{[11]}\sim E^{[11]}$. When $E^{[11]}>E_C^{[11]}\sim 4.283$, parameters $P^{[11]}$, $\eta_{11}^{[11]}$, and $d_{33}^{[11]}$ as a function of $E^{[11]}$, respectively, behave in the same way as the case of the NF lattice. Note here that peak II is ~76% higher than the peak I for the NL lattice, which represents a remarkable enhanced piezoelectric response in the RF lattice. What should be mentioned is that the window from $E_B^{[11]}$ to $E_C^{[11]}$ will be shifted leftward slightly with increasing defect concentration C_0, and this enhanced effect can be modulated by adjusting parameters b_M, C_0, and C_p, which will be reported elsewhere.

In summary, we have simulated the domain patterns, polarization, and piezoelectric behaviors of a RF lattice by numerically solving the TDGL equation based on the dipole defect model. An alternative origin of the enhanced piezoelectric response along the NSP axis has been proposed, which deals with the 90° flip of small-sized superferroelectric regions embedded in the matrix of coarse stripe domains. It is believed that this model reasonably explains the recently observed enhanced piezoelectric performance of some relaxor ferroelectrics as formed by doping the NF systems.

The authors acknowledge the support from the Natural Science Foundation of China (50332020 and 10021001) and National Key Projects for Basic Research of China (2002CB613303 and 2006CB921802). One of the authors (J.-M.L.) would like to acknowledge the hospitality of Boston College (Ren group) with which this work was completed.

[1] S.-E. Park and T. R. Shrout, J. Appl. Phys. **82**, 1804 (1997).
[2] H. X. Fu and E. Cohen, Nature (London) **403**, 281 (2000).
[3] R. S. Nasar, M. Cerqueira, E. Longo, E. R. Leite, A. J. Varela, A. Beltran, and J. Andres, J. Mater. Sci. **34**, 3659 (1999).
[4] W. Gong, J. F. Li, X. C. Chu, Z. L. Gui, and L. T. Li, Appl. Phys. Lett. **85**, 3818 (2004).
[5] G. Singh, I. Bhaumik, S. Ganesamoorthy, A. K. Karnal, and V. S. Tiwari, Mater. Lett. **60**, 3307 (2006).
[6] X. M. Wang, X. G. Tang, J. Wang, H. L. W. Chan, C. L. Choy, and H. S. Luo, Appl. Phys. Lett. **84**, 4711 (2004).
[7] S. Priya and K. Uchino, Jpn. J. Appl. Phys., Part 1 **42**, 531 (2003).
[8] S. Priya and K. Uchino, J. Appl. Phys. **91**, 4515 (2002).
[9] D. Kobor, L. Lebrun, G. Sebald, and D. Guyomar, J. Cryst. Growth **275**, 580 (2005).
[10] S. J. Zhang, L. Lebrun, C. A. Randall, and T. R. Shrout, J. Cryst. Growth **267**, 204 (2004).
[11] S. Priya and K. Uchino, Appl. Phys. Lett. **81**, 2430 (2002).
[12] Y. Sata, S. Abe, R. Fujimura, H. Ono, K. Oda, T. Shimura, and K. Kuroda, J. Appl. Phys. **96**, 4852 (2004).
[13] A. P. Levanyuk and A. S. Sigov, *Defects and Structural Phase Transitions* (Gordon and Breach, New York, 1988), p. 24.
[14] S. Semenovskaya and A. G. Khachaturyan, J. Appl. Phys. **83**, 5125 (1998).
[15] C. H. Park and D. J. Chadi, Phys. Rev. B **57**, 13961 (1998).
[16] J.-M. Liu, X. Wang, H. L. W. Chan, and C. L. Choy, Phys. Rev. B **69**, 094114 (2004).
[17] L. F. Wang and J.-M. Liu, Appl. Phys. Lett. **89**, 092909 (2006).
[18] J. B. Keith and D. M. Hatch, J. Appl. Phys. **100**, 033526 (2006).
[19] R. Ahluwalia, T. Lookman, A. Saxena, and W. Cao, Phys. Rev. B **72**, 014112 (2005).